GEOPHYSICS, VOL. 64, NO. 3 (MAY-JUNE 1999); P. 691–700, 8 FIGS., 2 TABLES.

Estimation of near-surface shear-wave velocity by inversion of Rayleigh waves

Jianghai Xia*, Richard D. Miller*, and Choon B. Park*

ABSTRACT

The shear-wave (*S*-wave) velocity of near-surface materials (soil, rocks, pavement) and its effect on seismic-wave propagation are of fundamental interest in many groundwater, engineering, and environmental studies. Rayleigh-wave phase velocity of a layered-earth model is a function of frequency and four groups of earth properties: *P*-wave velocity, *S*-wave velocity, density, and thickness of layers. Analysis of the Jacobian matrix provides a measure of dispersion-curve sensitivity to earth properties. *S*-wave velocities are the dominant influence on a dispersion curve in a high-frequency range (>5 Hz) followed by layer thickness. An iterative solution technique to the weighted equation proved very effective in the high-frequency range when using the Levenberg–Marquardt and singular-value decomposition techniques. Convergence of the weighted solution is guaranteed through selection of the damping factor using the Levenberg–Marquardt method. Synthetic examples demonstrated calculation efficiency and stability of inverse procedures. We verify our method using borehole *S*-wave velocity measurements.

INTRODUCTION

Elastic properties of near-surface materials and their effects on seismic-wave propagation are of fundamental interest in groundwater, engineering, and environmental studies. *S*-wave velocity is one of the key parameters in construction engineering. For example, Imai and Tonouchi (1982) studied *P*- and *S*-wave velocities in an embankment and also in alluvial, diluvial, and Tertiary layers, showing that *S*-wave velocities in such deposits correspond to the *N*-value (Craig, 1992), an index value of formation hardness used in soil mechanics and foundation engineering.

Surface waves are guided and dispersive. Rayleigh (1885) waves are surface waves that travel along a free surface, such as the earth–air interface. Rayleigh waves are the result of interfering *P*- and S_v-waves. Particle motion of the fundamental mode of Rayleigh waves moving from left to right is elliptical in a counterclockwise (retrograde) direction. The motion is constrained to the vertical plane that is consistent with the direction of wave propagation. Longer wavelengths penetrate deeper than shorter wavelengths for a given mode, generally exhibit greater phase velocities, and are more sensitive to the elastic properties of the deeper layers (Babuska and Cara, 1991). Shorter wavelengths are sensitive to the physical properties of surficial layers. For this reason, a particular mode of surface wave will possess a unique phase velocity for each unique wavelength, leading to the dispersion of the seismic signal.

S-wave velocity can be derived from inverting the dispersive phase velocity of the surface (Rayleigh and/or Love) wave (Dorman and Ewing, 1962; Aki and Richards, 1980; Mari, 1984). For the case of a solid homogeneous half-space, the Rayleigh wave is not dispersive and travels with a velocity of approximately $0.9194v$, if Poisson's ratio is equal to 0.25, where v is the *S*-wave velocity in the half-space (Sheriff and Geldart, 1982). However, in the case of one layer on the top of a solid homogeneous half-space, the Rayleigh wave disperses when its wavelengths are in the range of 1 to 30 times the layer thickness (Stokoe et al., 1994). Stokoe et al. (1994) also show that the Rayleigh wave travels with a velocity of approximately $0.9194v_1$ (where v_1 is the *S*-wave velocity of the layer) when the wavelengths of the Rayleigh wave are less than the layer thickness. At wavelengths greater than 30 times the layer thickness, the Rayleigh-wave phase velocity is approximately equal to $0.9194v_2$ (where v_2 is the *S*-wave velocity of the half-space).

Ground roll is a particular type of Rayleigh wave that travels along or near the ground surface and is usually characterized by relatively low velocity, low frequency, and high amplitude (Sheriff, 1991). Stokoe and Nazarian (1983) and Nazarian et al. (1983) present a surface-wave method called spectral analysis of surface waves (SASW) that analyzes the dispersion curve of ground roll to produce near-surface *S*-wave velocity profiles. SASW has been widely applied to many engineering projects (e.g., Sanchez-Salinero et al., 1987; Sheu et al., 1988; Stokoe

Manuscript received by the Editor May 1, 1997; revised manuscript received November 13, 1998.
*Kansas Geological Survey, 1930 Constant Ave., Lawrence, Kansas 66047-3726. E-mail: jxia@kgs.ukans.edu; rmiller@kgs.ukans.edu; cpark@kgs.ukans.edu.

et al., 1989; Gucunski and Woods, 1991; Hiltunen, 1991; Stokoe et al., 1994).

Inversion of dispersion curves to estimate *S*-wave velocities deep within the earth was first attempted by Dorman and Ewing (1962). Song et al. (1989) relate the sensitivity of model parameters to several key earth properties by modeling and present two real examples using surface waves to obtain *S*-wave velocities. Turner (1990) examines the feasibility of inverting surface waves (Rayleigh and Love) to estimate *S*-wave and *P*-wave velocity. Dispersion curves are inverted using least-squares techniques in SASW methods (Nazarian et al., 1983; Stokoe and Nazarian, 1983). Rix and Leipski (1991) examine the influence of the number of dispersion points, the maximum wavelength, and distribution of dispersion data with wavelength on the accuracy and resolution of *S*-wave velocity profiles.

The Kansas Geological Survey conducted a three-phase research project to estimate near-surface *S*-wave velocity from ground roll:

1) acquire high-frequency (≥5 Hz) broadband ground roll,
2) create efficient and accurate algorithms organized in a basic data processing sequence designed to extract Rayleigh-wave dispersion curves from ground roll, and
3) develop stable and efficient inversion algorithms to obtain near-surface *S*-wave velocity profiles.

The first two phases, acquisition of broadband ground roll and extraction of dispersion curves, are crucial to successfully estimate *S*-wave velocity through inversion. For phase 1, Park et al. (1996) introduce the multichannel analysis of surface waves using vibroseis (MASWV) method, which successfully produces broadband ground roll. Phase 2 results in a presentation by Park et al. (1998) demonstrating the cross-correlation of stacked amplitudes with sweep (CCSAS) technique, which can efficiently extract accurate Rayleigh-wave phase velocities from ground roll.

Analysis of the Jacobian matrix demonstrates that the sensitivity of earth properties to the dispersion curve is fundamental to understanding and determining the accuracy of an *S*-wave velocity model. Iterative solutions of a weighted damping equation using the Levenberg–Marquardt (L-M) method (Levenberg, 1944; Marquardt, 1963) provide a fast, stable solution. Calculation efficiency is achieved by reconstructing a weighted damping solution using the singular-value decomposition technique (Golub and Reinsch, 1970). Stability of the inverse procedure is guaranteed by selecting the appropriate damping factor in the L-M method.

METHOD

Consideration on numerical calculations

For a layered earth model (Figure 1), Rayleigh-wave dispersion curves can be calculated by Knopoff's method (Schwab and Knopoff, 1972). Rayleigh-wave phase velocity, c_{Rj}, is determined by a characteristic equation F in its nonlinear, implicit form:

$$F(f_j, c_{Rj}, \mathbf{v}_s, \mathbf{v}_p, \boldsymbol{\rho}, \mathbf{h}) = 0 \qquad (j = 1, 2, \ldots, m), \quad (1)$$

where f_j is the frequency, in Hz; c_{Rj} is the Rayleigh-wave phase velocity at frequency f_j; $\mathbf{v}_s = (v_{s1}, v_{s2}, \ldots, v_{sn})^T$ is the *S*-wave velocity vector, with v_{si} the shear-wave velocity of the ith layer; n is the number of layers; $\mathbf{v}_p = (v_{p1}, v_{p2}, \ldots, v_{pn})^T$ is the compressional *P*-wave velocity vector, with v_{pi} the *P*-wave velocity of the ith layer; $\boldsymbol{\rho} = (\rho_1, \rho_2, \ldots, \rho_n)^T$ is the density vector, with ρ_i the density of the ith layer; and $\mathbf{h} = (h_1, h_2, \ldots, h_{n-1})^T$ is the thickness vector, with h_i the thickness of the ith layer. Given a set of model parameters ($\mathbf{v}_s$, $\mathbf{v}_p$, $\boldsymbol{\rho}$, and $\mathbf{h}$) and a specific frequency (f_j), the roots of equation (1) are the phase velocities. In this study, only the fundamental mode was considered. If the dispersion curve consists of m data points, a set of m equations in the form of equation (1) can be used to find phase velocities at frequencies f_j ($j = 1, 2, \ldots, m$) using the bisection method (Press et al., 1992).

Accuracy of the partial derivatives is key in determining modifications to the earth model parameters and dramatically affects convergence of the inverse procedure (Xia, 1986). The practical way to calculate the partial derivatives of equation (1) is by evaluating finite-difference values because equation (1) is in an implicit form. In this study, Ridder's method of polynomial extrapolation (Press et al., 1992) is used to calculate the partial derivative or Jacobian matrix during the inversion. For implicit functions in general, evaluating the accuracy of partial derivatives may not be possible because they are calculated using a finite-difference formula. We can, however, evaluate the accuracy of partial derivatives with respect to densities [equation (1)] since density relationships are shown in equation (1) in the form of ρ_{i+1}/ρ_i (Schwab and Knopoff, 1972). Mathematically, this property shows that the direction of the partial derivative vector with respect to density, $\mathbf{J}_\rho$, is perpendicular to $\boldsymbol{\rho}$. That is, $\mathbf{J}_\rho \cdot \boldsymbol{\rho} = 0$, where $\cdot$ denotes the dot production. The partial derivatives $\mathbf{J}_\rho$ calculated by Ridder's method can be checked for accuracy using this relationship. The accuracy of numerical derivatives can be evaluated using an earth model (Table 1). Numerical results indicate that the average relative error in the estimated elements of the Jacobian matrix is approximately 0.1% with at least three significant figures. Our experience shows that estimating the Jacobian matrix in

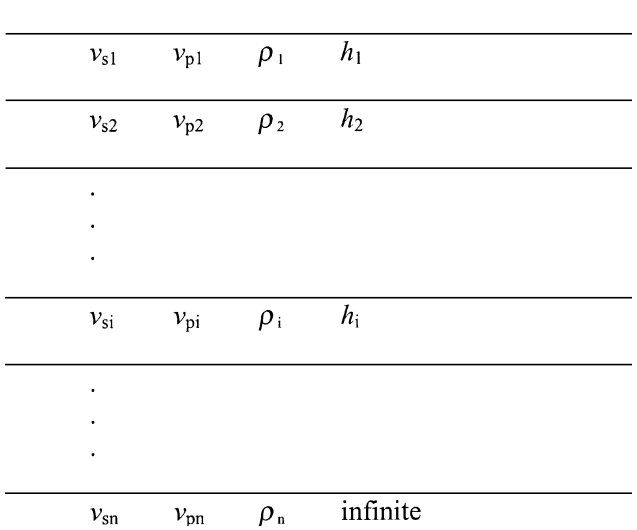

FIG. 1. A layered earth model with parameters of shear-wave velocity ($\mathbf{v}_s$), compressional wave velocity ($\mathbf{v}_p$), density ($\boldsymbol{\rho}$), and thickness ($\mathbf{h}$).

a high-frequency range (>5 Hz) by Ridder's method is stable. Most importantly, Ridder's method provides an efficient means to calculate the Jacobian matrix of the Rayleigh-wave phase velocity for the layered earth model. The other way to estimate the Jacobian matrix is to use variational techniques, which require computations of eigenfunctions but generate very stable estimates of partial derivatives (e.g., Aki and Richards, 1980, 290–292; Neigauz and Shkadinskaya, 1972).

Analysis of sensitivity of earth model parameters

Rayleigh-wave phase velocity (dispersion data) is the function of four parameters: *S*-wave velocity, *P*-wave velocity, density, and layer thickness [equation (1)]. Each parameter contributes to the dispersion curve in a unique way. A parameter can be negated from the inverse procedure if contributions to the dispersion curve from that parameter are relatively small in a certain frequency range. In this section, contributions to the Rayleigh-wave phase velocity in the high-frequency range (≥5 Hz) from each parameter are evaluated to determine which parameter can be inverted with reasonable accuracy.

Variations in *S*-wave velocities have a dramatic effect on Rayleigh-wave phase velocities. Using the same earth model as the previous model (Table 1), the Jacobian matrix of the model with respect to *S*-wave velocity $\mathbf{J}_S$ at frequencies f_j (=5, 10, 15, 20, 25, and 30 Hz) can be expressed as follows:

$$\mathbf{J}_S = \left[-\frac{\partial F/\partial v_{si}}{\partial F/\partial c_R}\bigg|_{f=f_j} \right] = \begin{bmatrix} 0.018 & 0.018 & 0.022 & 0.021 & 0.017 & 0.872 \\ 0.130 & 0.106 & 0.062 & 0.025 & 0.022 & 0.766 \\ 1.067 & 0.925 & 0.313 & 0.034 & 0.017 & 0.262 \\ 0.155 & 1.037 & 0.967 & 0.457 & 0.145 & 0.040 \\ 0.293 & 1.072 & 0.517 & 0.102 & 0.012 & 0.001 \\ 0.520 & 0.923 & 0.202 & 0.016 & 0.000 & 0.000 \end{bmatrix}. \quad (2)$$

Effects of changes in *S*-wave velocities on phase velocities can be calculated by multiplying $\mathbf{J}_S$ [equation (2)] with changes in *S*-wave velocities. Increasing *S*-wave velocities by 25% in the model (Table 1) results in a maximum difference of more than 250 m/s at $f = 20$ Hz or an average relative change of 39% in phase velocity. The effect on the phase velocity is represented by the differences in the solid line (phase velocities from the model of Table 1) and values represented by solid circles (phase velocities from model of Table 1 with 25% changes in *S*-wave velocity). Effects of the 25% increase in *S*-wave velocity are quite dramatic in comparison to similar changes in density or *P*-wave velocity (Figure 2). Numerical stability of a linear system can be presented by the condition number. The condition number of $\mathbf{J}_S^T\ \mathbf{J}_S$ is 5.6×10^5, which is an order of magnitude better than the condition number for the *P*-wave velocity model and two orders of magnitude better than the density solution shown as follows.

Table 1. Earth model parameters.

Layer number	$\mathbf{v}_s$ (m/s)	$\mathbf{v}_p$ (m/s)	ρ (g/cm^3)	**h** (m)
1	194.0	650.0	1.82	2.0
2	270.0	750.0	1.86	2.3
3	367.0	1400.0	1.91	2.5
4	485.0	1800.0	1.96	2.8
5	603.0	2150.0	2.02	3.2
Half-space	740.0	2800.0	2.09	Infinite

By analyzing matrix $\mathbf{J}_\rho$, the most sensitive data in terms of frequency are around 20 Hz. To maximize the effects of density variability (Table 1) on the dispersion curve, the first and second layers are decreased by 25% and the rest of the layers are increased by 25%. These changes in density represent approximately ±0.5 g/cm^3. In general, a 25% change in density is reasonable across a sand/shale, shale/limestone (Garland, 1979), and gravelly (or sand) soil/fire (or brick) clay (Carmichael, 1989) interface. Effects are shown in Figure 2. The average relative change in phase velocity between these two data sets is <10%.

Rayleigh-wave phase velocities are influenced much less by changes in *P*-wave velocities than by changes in density. A 25% increase in *P*-wave velocities (Table 1) represents a maximum difference of <20 m/s, or an average relative change of less than 3%. This significant change in compressional-wave velocity has a very subtle effect on the phase velocity (Figure 2).

The effect of layer thicknesses on Rayleigh-wave phase velocities can be minimized by dividing the subsurface into thinner and thinner layers within each unique and constant *S*-wave interval velocity. When the model (Table 1) defines a thickness increase of 25%, the average relative change in Rayleigh-wave phase velocities is approximately 16% (Figure 2).

Based on the analysis in previous paragraphs, we may conclude that the ratio of percentage change in the phase velocities to percentage change in the *S*-wave velocity, thickness of layer, density, or *P*-wave velocity is 1.56, 0.64, 0.4, or 0.13, respectively. The *S*-wave velocity is the dominant parameter influencing changes in Rayleigh-wave phase velocity for this

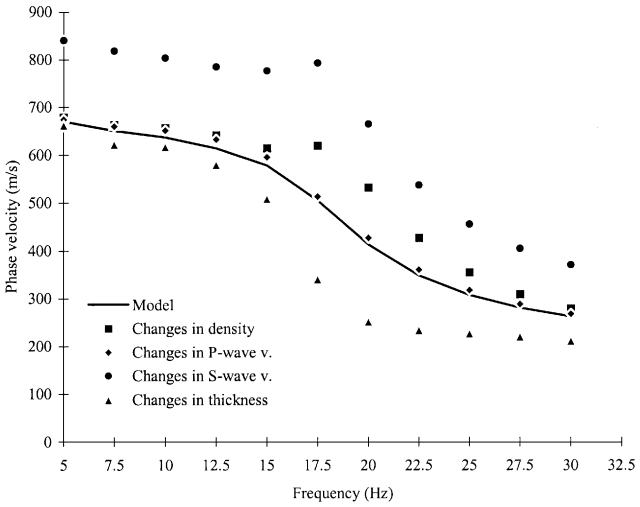

FIG. 2. Contributions to Rayleigh-wave phase velocity by 25% changes in each earth model parameter (Table 1). The solid line is Rayleigh-wave phase velocity attributed to the earth model listed in Table 1. Squares represent Rayleigh-wave phase velocities after 25% changes in density; diamonds represent Rayleigh-wave phase velocities after 25% changes in *P*-wave velocity, etc.

particular model in the high-frequency range (>5 Hz), which is therefore the fundamental basis for the inversion of *S*-wave velocity from Rayleigh-wave phase velocity. Analysis presented in this section is based on a single model (Table 1); however, numerical results from more than 100 modeling tests support these conclusions.

In summary, a 25% error in estimated *P*-wave velocity or rock density results in <10% difference between the modeled and actual dispersion curves. Since in the real world it is relatively easy to obtain density information with accuracy >25% (Carmichael, 1989), densities can be assumed known in our inverse procedure. It is also reasonable to suggest that relative variations in *P*-wave velocities can be estimated within 25% of actual; therefore, *P*-wave velocities will also be assumed known. Inverting Rayleigh-wave phase velocity for layer thickness is more feasible than for *P*-wave velocity or density because the sensitivity indicator is greater for thickness variation than for *P*-wave velocity or density. However, because the subsurface can always be subdivided into a reasonable number of layers, each possessing an approximatly constant *S*-wave velocity, thickness can be eliminated as a variable in our inverse procedure. Only *S*-wave velocities are left as unknowns. We can reduce the number of unknowns in equation (1) from $4n-1$ (where n is number of layers) to n with these assumptions. The fewer unknowns in an inverse procedure, the more efficient and stable the process and the more reliable the solutions.

Inversion algorithm

The basis was developed for suggesting that *S*-wave velocities fundamentally control changes in Rayleigh-wave phase velocities for a layered earth model in the previous section. Therefore, *S*-wave velocities can be inverted adequately from Rayleigh-wave phase velocities. In this section, we start with linearizing equation (1). Then we define an objective function and a weighting matrix, list a solution of minimizing the objective function by the L-M method and the SVD technique, and discuss formulas that determine initial values.

S-wave velocities (earth model parameters) can be represented as the elements of a vector $\mathbf{x}$ of length n, or $\mathbf{x} = [v_{s1}, v_{s2}, v_{s3}, \ldots, v_{sn}]^T$. Similarly, the measurements (data) of Rayleigh-wave phase velocities at m different frequencies can be represented as the elements of a vector $\mathbf{b}$ of length m, or $\mathbf{b} = [b_1, b_2, b_3, \ldots, b_m]^T$. Since the model $\mathbf{c}_R$ [equation (1)] is a nonlinear function, equation (1) must be linearized by Taylor-series expansion to employ the matrix theory:

$$\mathbf{J}\Delta\mathbf{x} = \Delta\mathbf{b}, \tag{3}$$

where $\Delta\mathbf{b} = \mathbf{b} - \mathbf{c}_R(\mathbf{x}_0)$ and is the difference between measured data and model response to the initial estimation, in which $\mathbf{c}_R(\mathbf{x}_0)$ is the model response to the initial *S*-wave velocity estimates, $\mathbf{x}_0$; $\Delta\mathbf{x}$ is a modification of the initial estimation; and $\mathbf{J}$ is the Jacobian matrix with m rows and n columns ($m > n$). The elements of the Jacobian matrix are the first-order partial derivatives of $\mathbf{c}_R$ with respect to *S*-wave velocities.

Since the number of data points contained in the dispersion curve is generally much larger than the number of layers used to define the subsurface ($m > n$), equation (3) is usually solved by optimization techniques. We defined the objective function as

$$\Phi = \|\mathbf{J}\Delta\mathbf{x} - \Delta\mathbf{b}\|_2\mathbf{W}\|\mathbf{J}\Delta\mathbf{x} - \Delta\mathbf{b}\|_2 + \alpha\|\Delta\mathbf{x}\|_2^2, \tag{4}$$

where $\| \|_2$ is the ℓ_2-norm length of a vector, α is the damping factor, and $\mathbf{W}$ is a weighting matrix. This is a constrained (weighted) least-squares problem. We are searching for a solution with minimum modification to model parameters so the convergence procedure is stable for each iteration. This does not mean the final model will be closer to the initial model than other optimization techniques such as the Newton method. After several iterations, the sum of the modifications is added to the initial model, making a final model that can be significantly different from the initial model as shown in the synthetic example (see Figure 4).

The Jacobian matrix $\mathbf{J}_S$ [equation (2)] allows comparison of the change rates in Rayleigh-wave phase velocity with respect to *S*-wave velocity within different layers at different frequencies (data points). Row vectors of the Jacobian matrix represent the rate of change in the Rayleigh-wave phase velocity as a function of the *S*-wave velocity within defined layers for specific frequencies. The length of the row vectors of the Jacobian matrix $\mathbf{J}_S$ [equation (2)] indicates the maximum value (1.505) at 20 Hz, which is the frequency with the highest resolution for this particular model (Table 1). Vector $\mathbf{s}$ also shows that data from 15 to 25 Hz contain the greatest resolution. Therefore, this frequency portion of dispersion data should be weighted heavier than data at other frequencies during inversion. The weighting matrix for our inversion is based on differences in Rayleigh-wave phase velocities with respect to frequency. Since the weighting matrix $\mathbf{W}$ [equation (4)] is both diagonal and positive, we can write $\mathbf{W} = \mathbf{L}^T\mathbf{L}$, where $\mathbf{L}$ is also a diagonal matrix.

Marquardt (1963) points out that the damping factor controls the direction of $\Delta\mathbf{x}$ and the speed of convergence. The damping factor also acts as a constraint on the model space (Tarantola, 1987, chapter 4). By adjusting the damping factor, we can improve processing speed and guarantee the stable convergence of the inversion. In practice, several different values of α need to be tried to find a proper damping factor. Using the singular-value decomposition technique to minimize the objective function (4) allows us to change the damping factor without recalculating the inverse matrix of $(\mathbf{A}^T\mathbf{A} + \alpha\mathbf{I})$, where $\mathbf{A} = \mathbf{LJ}$. The solution is

$$\Delta\mathbf{x} = \mathbf{V}(\mathbf{\Lambda}^2 + \alpha\mathbf{I})^{-1}\mathbf{\Lambda}\mathbf{U}^T\mathbf{d}, \tag{5}$$

where matrix $\mathbf{A}$ is decomposed as $\mathbf{A} = \mathbf{U}\mathbf{\Lambda}\mathbf{V}^T$, $\mathbf{d} = \mathbf{Lb}$, and $\mathbf{I}$ is the unit matrix.

The resolution of the inverse results as calculated by equation (5) is difficult to determine because the general inverse matrix $[\mathbf{V}(\mathbf{\Lambda}^2 + \alpha\mathbf{I})^{-1}\mathbf{\Lambda}\mathbf{U}^T]$ is a function of the damping factor. Model parameters can be completely resolved only when the damping factor is equal to zero. On the other hand, variance in model parameters increases as the damping factor decreases. In practice, resolution of model parameters can be analyzed by minimizing the trade-off curve between resolution and variance. For our test model, the damping factor rapidly approaches zero when an inverted model converges to the true model.

The Jacobian matrix [equation (2)] also suggests phase-velocity data as a function of frequency possess different resolving powers for determining *S*-wave velocities at different depths. Each column vector of the Jacobian matrix [equation (2)] shows the sensitivity of different dispersion data. For

example, the maximum value (1.067) in the first column indicates Rayleigh-wave phase velocity at 15 Hz has the greatest resolving power to determine the *S*-wave velocity of the first layer. The second column shows dispersion data between 15 and 25 Hz possess the most information about the *S*-wave velocity of the second layer. The last column suggests data from 5 to 10 Hz contain most of the information about the *S*-wave velocity of the half-space. Based on these observations, it is reasonable to use Rayleigh-wave phase velocities selectively at specific frequencies to define initial depth-dependent *S*-wave velocities. In our iterative procedure, initial *S*-wave velocities are determined using the following formulas:

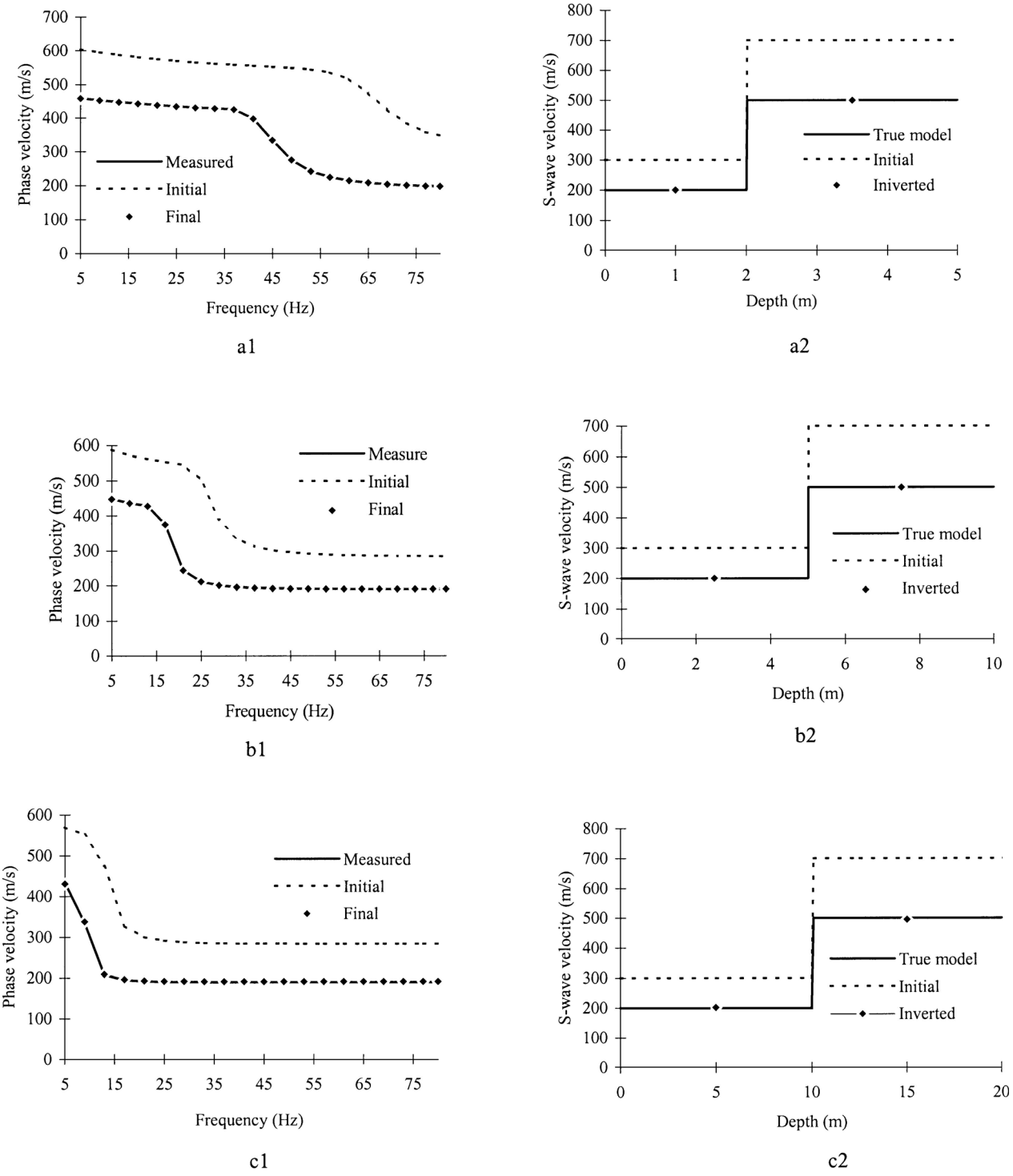

FIG. 3. Inversion results of two-layer models. Initial models are about 50% off true models in these three cases. Dispesion curves (a1, b1, and c1) labeled as Measured, Initial, and Final are phase-wave velocities from the True, Initial, and Inverted models (a2, b2, and c2), respectively. One of every four phase velocities attributed to the inverted model is marked by diamonds (a1, b1, and c1).

$$v_{s1} = c_R(\text{high})/\beta \quad \text{(for the first layer)},$$
$$v_{sn} = c_R(\text{low})/\beta \quad \text{(for the half-space), and} \quad (6)$$
$$v_{si} = c_R(f_i)/\beta, \quad (i = 2, 3, \ldots, n-1),$$

where β is a constant ranging from 0.874 to 0.955 for Poisson's ratio ranges from 0.0 to 0.5 (Stokoe et al., 1994). Based on our modeling studies, β is chosen as 0.88. Asymptotic approximations of Rayleigh-wave phase velocities within the higher frequency range c_R(high) and the lower frequency range c_R(low) are defined when the measured dispersion curve clearly shows asymptotes on both ends. If the asymptotes do not show up on the dispersion curve, the highest and lowest phase velocities can be chosen as c_R(high) and c_R(low), respectively.

For layers between the first layer and half-space, a certain wavelength of Rayleigh wave is selected for a given layer based on the fact that a different wavelength of Rayleigh wave has a different maximum penetration depth. Our modeling results suggest Rayleigh-wave velocity $c_R(f_i)$ with a wavelength (L) can be used in equation (6) to find the initial values for the S-wave velocity of the layer at a depth of $0.63L$. The initial values of S-wave velocities determined in this way may not be the best, but they are good enough to start the inversion algorithm. During hundreds of modeling tests, initial values determined by equation (6) always converged to true models.

Two-layer modeling results suggest it is difficult to determine the depth to the half-space based on the dispersion curve alone because it is strongly dependent on the S-wave velocity of the half-space. It appears that one-half of the longest wavelength of the Rayleigh waves is optimum as the maximum depth to the half-space.

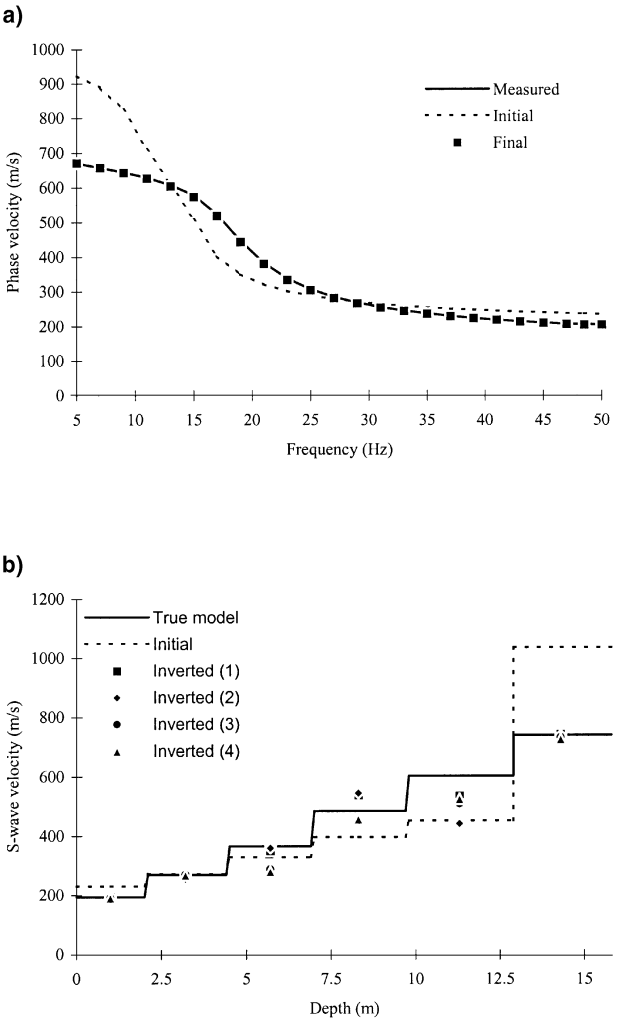

FIG. 4. Inversion results of multilayer examples. Labels on dispersion curves (a) and S-wave velocity profiles (b) have the same meaning as labels in Figure 3. The true model (b) is listed in Table 1. The initial model (b) except for the S-wave velocity of the half-space shown by the dashed line was calculated based on equation (6). Four inverted models (b) marked by different symbols were the final models of four cases from our inverse procedure. One of every two phase velocities attributed to the inverted model is shown by squares (a).

SYNTHETIC EXAMPLES

Two-layer models

The same two-layer models as previously used (Figure 3) will help to examine the inversion algorithm. Initial S-wave velocities are 300 and 700 m/s for the layer and half-space, respectively. By design, these values are approximately 50% off the true values. For the 2-m model (Figures 3a1 and 3a2), the rms error is reduced from 201 to 0.7 m/s after four interations. For the 5-m model (Figures 3b1 and 3b2), the rms error is reduced from 149 to 0.3 m/s after four iterations. For the 10-m model (Figures 3c1 and 3c2), the rms error is reduced from 123 to 1.5 m/s after three iterations. For these three simple models, the shear-wave velocities are exactly inverted. In practice, two-layer models may be useful for estimation of static correction (Mari, 1984).

Multilayer models

The multilayer model (Table 1) is used to examine efficiency and stability of the inversion algorithm and to evaluate effects of errors in the P-wave velocity and/or density on the inverted S-wave velocity. Model parameters (Table 1) of synthetic examples are inverted with different initial models. Initial S-wave velocities for all layers of the models except the half-space are determined using equation (6) (230.8, 272.2, 330.5, 396.5, and 453.0 m/s from layer one to layer five, respectively). The initial estimate of the S-wave velocity for the half-space is 1036 m/s, which is 40% off the true value. For case 1, P-wave velocities and densities are consistent with the true model (Table 1). The final rms error between phase velocities calculated from the true model and the inverted model was reduced from 89 to 2 m/s. Constraints to minimize the modification of S-wave velocities for each iteration are applied to all layers and the half-space. The inversion results (=initial velocities plus a summation of all modifications) clearly suggest the inverted results do not need to be close to the initial estimates. The final S-wave velocity of the half-space for this example is improved by 40% from its initial estimate.

In the real world, estimated errors in P-wave velocities, density, and thickness of layers always exist. In the following examples, the inverted results of v_s show the effects of errors in the estimates of P-wave velocity and/or density. Let us consider case 2 when the initial S-wave velocities and measured data are the same as case 1 but the P-wave velocities change up to

25% relative to the true model (Table 1). Values of v_p are 812.5, 937.5, 1750.0, 2250.0, 2687.0, and 3500.0 m/s from the top layers to the half-space, respectively. The inverted results of v_s will be affected by the errors in P-wave velocity (Figure 4b). For case 3, the initial S-wave velocities and measured data are the same as case 1 but the densities change up to 25% relative to the true model (1.32, 1.36, 2.41, 2.46, 2.52, and 2.59 g/cm^3 from the top layers to the half-space, respectively). The inverted results of v_s must be affected by the errors in density (Figure 4b). Finally, let us consider case 4 when the initial S-wave velocities and measured data are the same as case 1 but both P-wave velocities and densities change up to 25% relative to the true model. The phase velocities resulting from the inverted model of the last three cases are not shown in Figure 5a because they are very close to the phase velocities of the inverted model of case 1.

The overall average error between the inverted v_s and the true v_s is 4.4% for the case where is no error in P-wave velocities or densities and 8% for the other cases which include errors in P-wave velocity, density, and a combination. In all these cases, S-wave velocities for layer 1, layer 2, and the half-space are well resolved. The maximum error occurs at layer 3 of case 4, which is 23%. Maximums of four iterations were used for all these examples. Total processing time is less than 1 minute on a PC with a Pentium processor. For the last three cases, we stopped iterating when the rms errors dropped from the initial rms error of about 100 to 15 m/s because there are errors in P-wave velocities and/or densities of the models.

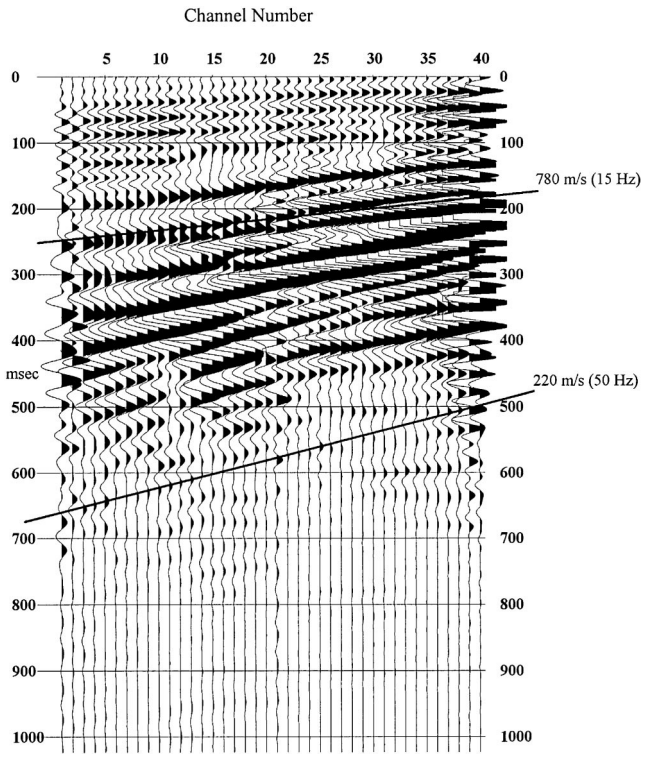

FIG. 5. The field data acquired near the Kansas Geological Survey during the winter of 1995. Forty groups of 10-Hz geophones were spread 1 m apart. An IVI MiniVib was used as the energy source and was located 27 m away from the right side of the geophone spread. Two linear events are velocities of dispersive ground roll at frequencies of approximately 15 and 50 Hz.

A REAL-WORLD EXAMPLE

Surface-wave data were acquired during the winter of 1995 near the Kansas Geological Survey in Lawrence, Kansas, using the MASWV acquisition method (Park et al., 1996). An IVI MiniVib was used as the energy source. Forty groups of 10-Hz geophones were deployed on 1-m intervals, with the first group of geophones 2 m from a test well. The source was located adjacent to the geophone line relative to the test well with a nearest source offset of 27 m. A 10-s linear upsweep with frequencies ranging from 10 to 200 Hz was generated for each shot station. The raw filed data acquired by the MASWV method possess a strong ground roll component (Figure 5). The two linear events on this shot gather define the range of phase velocities of the dispersive ground roll. The dispersion curve (Figure 6a) of Rayleigh-wave phase velocities has been extracted from filed data (Figure 5) for frequencies ranging from 15 to 80 Hz using CCSAS processing techniques (Park et al., 1998).

Three-component borehole data were acquired coincidentally to obtain P-wave and S-wave velocity vertical profiles. A cross-correlation technique was used to confidently determine S-wave arrivals on the recorded three-component borehole data. Any error on the S-wave velocity profile (the solid line in Figure 6b) is mainly because of the 0.5-ms sampling interval. The overall error in S-wave velocity of the borehole survey is approximately 10%.

Inverting the Rayleigh-wave phase velocities to determine S-wave velocities requires that densities and P-wave velocities be defined. Densities were estimated and designated to increase approximately linearly with depth, while P-wave velocities were obtained from borehole data (Table 2). The initial S-wave model (Initial B curve, Figure 6) was created by the inverse program based on equation (6). The rms error between measured data and modeled data dropped from 70 to 30 m/s with two iterations. The inverted S-wave velocity profile is horizontally averaged across the length of the source-geophone spread (66 m). Theoretically, considering this averaging, there should be only small differences between inverted velocity and borehole measured velocity. The average relative difference between inverted S-wave velocities and borehole-measured S-wave velocities is 18%. If the first layer is excluded, the difference is only 9%.

To analyze the sensitivity of the inverted model to initial values, we manually select initial values for v_s that are uniformly greater than borehole values (Figure 6). Initial A and Initial B curves are symmetrical to the borehole values and converge to borehole values from two different directions (Figure 6b).

Table 2. The initial model of the real example.

Layer number	$\mathbf{v}_s$ (m/s)	$\mathbf{v}_p$ (m/s)	ρ (g/cm^3)	**h** (m)
1	167.736	534.0	1.820	1.0
2	254.305	536.0	1.860	2.0
3	367.060	791.0	1.91	3.1
4	425.016	1212.0	1.96	3.1
5	472.324	1460.0	2.02	3.0
6	558.080	2400.0	2.09	4.6
7	672.877	2306.0	2.17	4.6
8	813.468	2226.0	2.26	6.0
9	813.468	2531.0	2.35	6.1
10	852.274	2410.0	2.4	Infinite

Overall accuracy for both inverted models is visually the same. Some confidence in the inverted model can be obtained from observing that both initial models approach borehole results, especially for the shallower part of the vertical profile (<20 m).

Initial value selections are critical to the convergence of the inversion results if an unrealistic or excessive range of initial velocity values is chosen. To verify this suggestion, the following test was formulated. For an initial model with a uniform constant-velocity half-space, a variety of solutions result from a constant initial velocity ranging from 100 to 1800 m/s (Figure 7). The inverted results of these blindly selected initial values converge to borehole results. The total number of iterations is less than 20 in each case. For initial values of 50 or 1900 m/s, the inversion did not converge. In the real world, however, extreme values such as 50 or 1900 m/s would not be a potential candidate for initial values if the Rayleigh-wave phase velocities are used to constrain the range of possible v_s values.

The number of data points (phase velocity versus frequency) will not have a significant influence on inversion results as long as a wide enough range of wavelengths has uniformly encountered the depths of interest. Using Figure 6, it is possible to study the inversion results from different sets of phase velocities (Figure 8). Comparing inversion results with 33, 17, and 66 data points (solid circles in Figure 8), there appears to be no decrease in accuracy because of reductions in the number

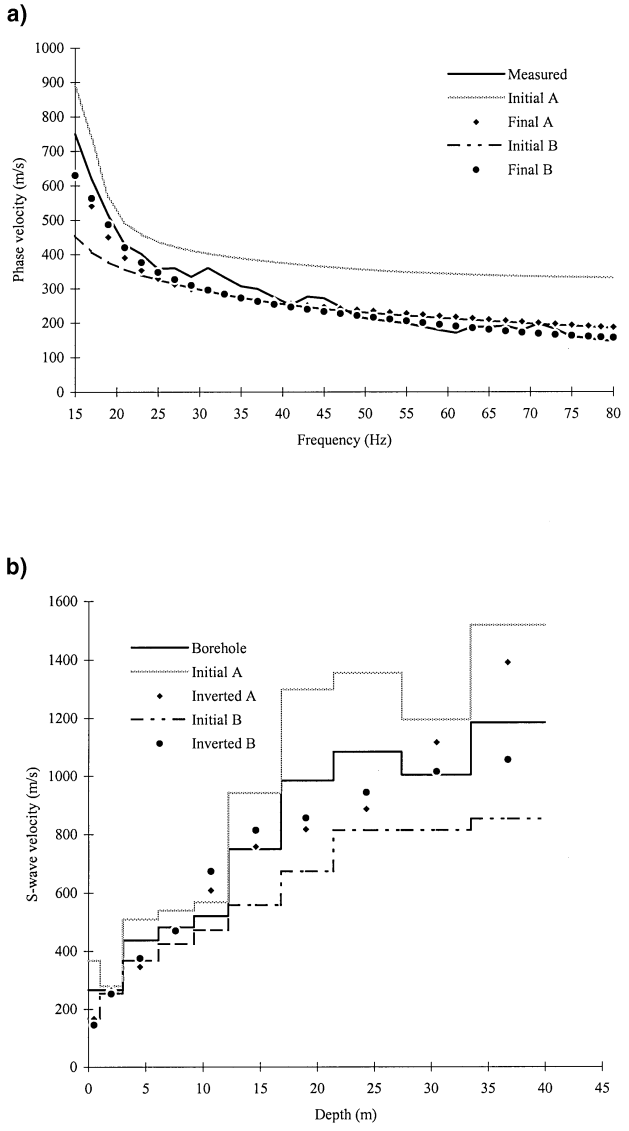

FIG. 6. Inverse results of the real example. Labels on dispersion curves (a) and *S*-wave velocity profiles (b) have the same meaning as in labels Figure 4, except that the dispersion curve labeled measured (a) is real data extracted from filed data (Figure 5) by CCSAS techniques (Park et al., 1998). Initial B model (b) was calculated from the measured data in (a) based on equation (6). Borehole (b) was *S*-wave velocities derived from the three-component seismic borehole survey. Initial A and Initial B models (b) are symmetrical to the borehole values. Both initial models converge to the model determined by borehole data. One of every two phase velocities attributed to the inverted models is shown by diamonds and dots (a).

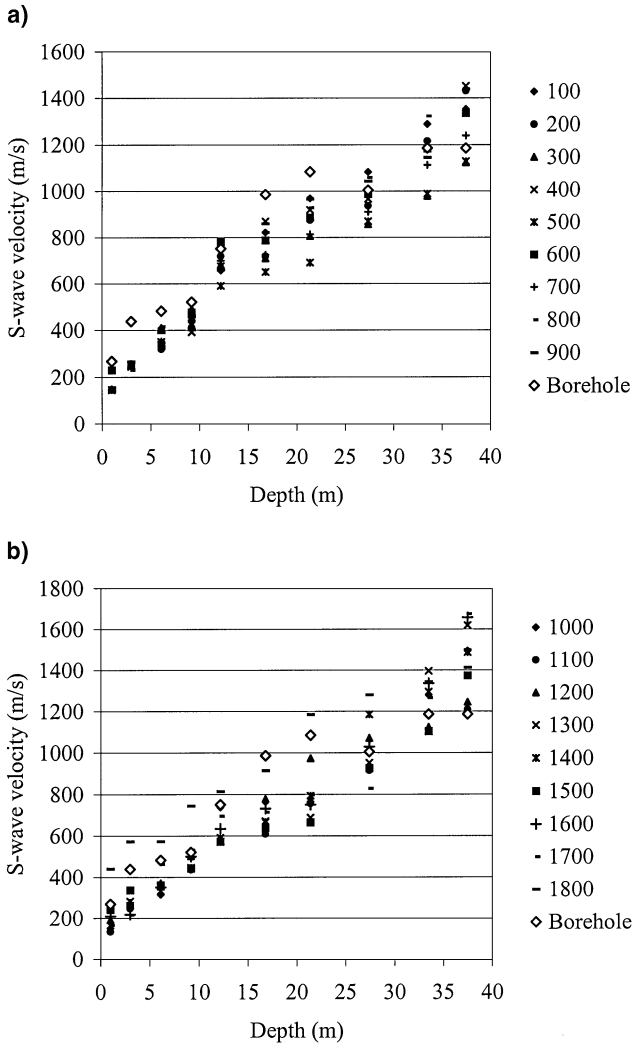

FIG. 7. Inversion results of phase velocities shown in Figure 6a started from a uniform half-space with a constant *S*-wave velocity. (a) Constant initial values are blindly selected from 100 to 900 m/s. For example, the solid diamonds indicate the inverted results from the initial model listed in Table 2, except the second column (v_s) is replaced by 100 m/s for all layers. (b) Constant initial values are blindly selected from 1000 to 1800 m/s.

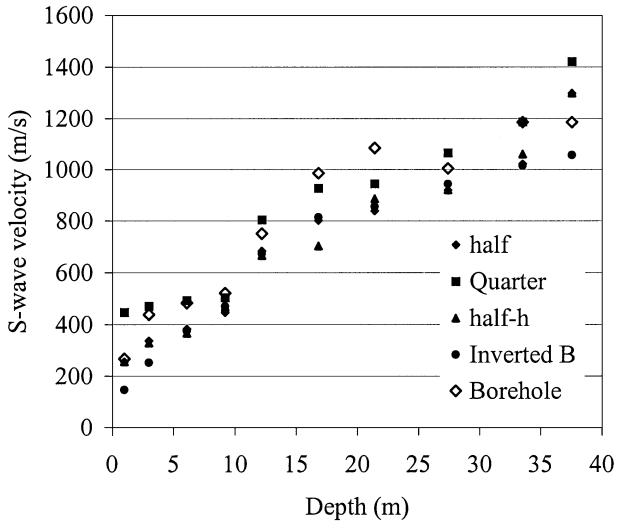

FIG. 8. Effect of the number of data points on inversion results. The solid diamonds indicate the inversion results from data points from 15 to 47 Hz (33 points); solid squares, 15 to 31 Hz (17 points); solid triangles, 15 to 47 Hz with an interval of 2 Hz (17 points); and solid circles, 15 to 80 Hz.

of data points. A single octave of data (15 to 31 Hz) still results in a good inversion. These results are consistent with previous findings (Rix et al., 1991).

The utility of this technique over borehole measurements becomes obvious when comparing the accuracy of the inverted velocity profile from the borehole measured velocity profile at associated costs and environmental risks. Permitting, drilling, and completing a borehole to 30 m has a wide range of potential expenses that are strongly dictated by where and when the borehole is planned. For this comparison, the cost of acquiring borehole velocities is estimated for an area with no governmental or residential constraints, no permitting requirements, and no environmental concerns. In an unconsolidated setting, installation of a borehole accessible to a three-component hole-locking receiver costs about $30 to $40 per meter plus mobilization, which generally runs around $1000 for a local crew. Acquiring velocity measurements in a 30-m-deep borehole generally requires about 4 hours for a two-person crew, running about $500. For this example, processing costs of the surface-wave data and borehole velocity data and crew mobilization are considered equal. Acquiring surface-wave data sufficient to produce a high-quality shear-wave velocity profile requires 2 hours for two people at most sites including setup and breakdown, costing around $250. Based on these figures, it costs about an order of magnitude more for a borehole-measured, shear-wave velocity profile than a surface-wave inversion shear-wave velocity profile. This represents the best-case scenario for the borehole-measured velocity profile. Routinely, health and environmental concerns play a major role that potentially could run up the cost of a borehole measure by orders of magnitude.

CONCLUSIONS

Inverting high-frequency Rayleigh-wave dispersion data can provide reliable near-surface *S*-wave velocities. Through analysis of the Jacobian matrix, we can begin to quantitatively sort out some answers to questions about the sensitivity of Rayleigh-wave dispersion data to earth properties. For a layered earth model defined by *S*-wave velocity, *P*-wave velocity, density, and thickness, *S*-wave velocity is the dominant property for the fundamental mode of high-frequency Rayleigh-wave dispersion data. In practice, it is reasonable to assign *P*-wave velocities and densities as known constants with a relative error of 25% or less. It is impossible to invert Rayleigh-wave dispersion data for *P*-wave velocity and density based on analysis of the Jacobian matrix for the model (Table 1). This is why poor results have previously been obtained by inverting Rayleigh waves to determine *P*-wave velocities (Turner, 1990). We have presented iterative solutions to the weighted equation by the L-M method and the SVD technique. Synthetic and real examples demonstrated calculation efficiency and stability of the inverse procedure. The inverse results of our real example are verified by borehole *S*-wave velocity measurements.

ACKNOWLEDGMENTS

The authors thank Joe Anderson, David Laflen, and Brett Bennett for their assistance during the field tests. The authors greatly appreciate thoughtful and constructive suggestions and critiques from Associate Editor Kurt Marfurt, Robert Herrmann, and one anonymous reviewer (Herrmann also confirmed our numerical Jacobian matrix by comparing with results calculated by variational techniques); the work is significantly improved because of it. The authors also appreciate the efforts of Marla Adkins-Heljeson and Mary Brohammer in manuscript preparation.

REFERENCES

Aki, K., and Richards, P. G., 1980, Quantitative seismology: W.H. Freeman & Co.
Babuska, V., and Cara, M., 1991, Seismic anisotropy in the earth: Kluwer Academic Publishers.
Carmichael, R. S., 1989, Practical handbook of physical properties of rocks and minerals: CRC Press, Inc.
Craig, R. F., 1992, Soil mechanics: Chapman and Hall.
Dorman, J., and Ewing, M., 1962, Numerical inversion of seismic surface wave dispersion data and crust-mantle structure in the New York–Pennsylvania area: J. Geophys. Res., **67**, 5227–5241.
Garland, G. D., 1979, Introduction to geophysics: Mantle, core and crust: W.B. Saunders Co.
Golub, G. H., and Reinsch, C., 1970, Singular value decomposition and least-squares solution: Num. Math., **14**, 403–420.
Gucunski, N., and Wood, R. D., 1991, Instrumentation for SASW testing, *in* Bhatia, S. K., and Blaney, G. W., Eds., Recent advances in instrumentation, data acquisition and testing in soil dynamics: Am. Soc. of Civil Engin., Geotechnical special publication no. **29**, 1–16.
Hiltunen, D. R., 1991, Nondestructive evaluation of pavement systems by the SASW method: Geotechnical News, **9**, September, 22–25.
Imai, T., and Tonouchi, K., 1982, Correlation of N-value with S-wave velocity: 2nd Euro. Symp. on Penetration Testing, Proceedings, 67–72.
Levenberg, K., 1944, A method for the solution of certain nonlinear problems in least squares: Quart. Appl. Math., **2**, 164–168.
Mari, J. L., 1984, Estimation of static correction for shear-wave profiling using the dispersion properties of Love waves: Geophysics, **49**, 1169–1179.
Marquardt, D. W., 1963, An algorithm for least squares estimation of nonlinear parameters: J. Soc. Indus. Appl. Math., **2**, 431–441.
Nazarian, S., Stokoe II, K. H., and Hudson, W. R., 1983, Use of spectral analysis of surface waves method for determination of moduli and thicknesses of pavement systems: Transport. Res. Record No. **930**, 38–45.
Neigauz, M. G., and Shkadinskaya, G. V., 1972, Method for calculating surface Rayleigh waves in a vertically inhomogeneous half-space,

in Keilis-Borok, V. I., Ed., Computational seismology: Plenum Press.
Park, C. B., Miller, R. D., and Xia, J., 1996, Multi-channel analysis of surface waves using Vibroseis (MASWV): 66th Ann. Internat. Mtg., Soc. Expl. Geophys., Expanded Abstracts, 68–71.
Park, C. B., Miller, R. D., and Xia, J., 1998, Imaging dispersion curves of surface waves on multi-channel record: 68th Ann. Internat. Mtg., Soc. Expl. Geophys., Expanded Abstracts, 1377–1380.
Press, W. H., Teukosky, S. A., Vetterling, W. T., and Flannery, B. P., 1992, Numerical recipes in C: Cambridge Univ. Press.
Rayleigh, L., 1885, On waves propagated along the plane surface of an elastic solid: Proc. Lon. Math. Soc., **17**, 4–11.
Rix, G. J., and Leipski, A. E., 1991, Accuracy and resolution of surface wave inversion, *in* Bhatia, S. K., and Blaney, G. W., Eds., Recent advances in instrumentation, data acquisition and testing in soil dynamics: Am. Soc. Civil Eng., Geotechnical Special Publication No. **29**, 17–23.
Sanchez-Salinero, I., Roesset, J. M., Shao, K. Y., Stokoe II, K. H., and Rix, G. J., 1987, Analytical evaluation of variables affecting surface wave testing of pavements: Transportation Res. Record No. **1136**, 86–95.
Schwab, F. A., and Knopoff, L., 1972, Fast surface wave and free mode computations, *in* Bolt, B. A., Ed., Methods in computational physics: Academic Press, 87–180.
Sheriff, R. E., 1991, Encyclopedic dictionary of exploration geophysics: Soc. Expl. Geophys.
Sheriff, R. E., and Geldart, L. P., 1985, Exploration seismology **I**: History, theory, and data acquisition: Cambridge Univ. Press.
Sheu, J. C., Stokoe II, K. H., and Roesset, J. M., 1988, Effect of reflected waves in SASW testing of pavements: Transportation Res. Record No. **1196**, 51–61.
Song, Y. Y., Castagna, J. P., Black, R. A., and Knapp, R. W., 1989, Sensitivity of near-surface shear-wave velocity determination from Rayleigh and Love waves: 59th Ann. Internat Mtg., Meeting, Soc. Expl. Geophys., Expanded Abstracts, 509–512.
Stokoe II, K. H., and Nazarian, S., 1983, Effectiveness of ground improvement from spectral analysis of surface waves: 8th Euro. Conf. on Soil Mech. and Found. Engin. Proceedings.
Stokoe II, K. H., Rix, G. J., and Nazarian, S., 1989, In situ seismic testing with surface wave: 12th Internat. Conf. on Soil Mechanics and Found. Engin. Proceedings, 331–334.
Stokoe II, K. H., Wright, G. W., Bay, J. A., and Roesset, J. M., 1994, Characterization of geotechnical sites by SASW method, *in* Woods, R. D., Ed., Geophysical characterization of sites: Oxford Publishers.
Tarantola, A., 1987, Inverse problem theory: Elsevier Science Publ. Co., Inc.
Turner, M. A., 1990, Near-surface velocity reconstruction using surface wave inversion: M.S. thesis, Univ. of Utah.
Xia, J., 1986, Some problems in interpretation of two-dimensional magnetic anomalies by nonlinear programming: Symp. of Geophys. and Geochem. Prosp., 174–187 (in Chinese).